JOURNAL OF APPLIED ELECTROCHEMISTRY 23 (1993) 887–896

Development of the flow-through porous electrode cell for bromide recovery from brine solutions

JIAN QI*, R. F. SAVINELL‡

Department of Chemical Engineering, Case Western Reserve University, Cleveland, Ohio 44106, USA

Received 26 April 1992; revised 8 January 1993

A continuous electrochemical process for bromine production from brine solutions was developed based on bromide oxidation and flow-through porous electrode technology. The bromide oxidation kinetics in a three-dimensional porous graphite electrode was determined using a small test flow cell. The data were analysed and combined into a process model to evaluate the electrode performance under many different operating conditions. Bromide conversions against cell sizes for various brine throughputs were calculated using model equations and verified by experimental data collected from a 45 cm long pilot cell.

Nomenclature

Symbols

a	electrochemical reaction area per unit volume electrode (cm^{-1})
C^0_{Br}	total Br content in anolyte (M)
C_{Br^-}	bromide concentration (M)
$C^1_{Br^-}$, $C^2_{Br^-}$	anode inlet and outlet bromide concentrations (M)
C_{BrCl}	BrCl concentration (M)
$C_{BrCl_2^-}$	$BrCl_2^-$ concentration (M)
C_{Cl^-}	chloride concentration (M)
C_{Cl_2}	aqueous chlorine concentration (M)
$C_{Cl_3^-}$	Cl_3^- concentration (M)
$C^1_{H^+}$	anode inlet proton concentration (M)
C_{HBrO}	HBrO concentration (M)
C^1_{HBrO}	anode inlet HBrO concentration (M)
C^1_{HClO}	anode inlet HClO concentration (M)
D	diffusion coefficient of bromide ($cm^2\ s^{-1}$)
F	Faraday's constant (96 485 C mol^{-1})
f	bromide conversion
f_{exp}	bromide conversion measured by experiments
f_{est}	bromide conversions predicted from theory
h_1, h_2, h_3	dimensionless terms representing, respectively, the effects contributed by incomplete chlorination, hydrolysis, and formation of BrCl
I	total cell current (mA)
^vI	cell volume current density (mA cm^{-3})
$^vI_{Cl^-}$	volume current density attributed to chloride oxidation (mA cm^{-3})
$^vI_{Br^-}$	volume current density attributed to bromide oxidation (mA cm^{-3})
I_{O_2}	water oxidation current (mA)
i_{Br^-}	bromide oxidation current density (mA cm^{-2})
i_{Cl^-}	chloride oxidation current density (mA cm^{-2})
i_{O_2}	water oxidation current density (mA cm^{-2})
K_1	equilibrium constant of Reaction R1, $= \dfrac{(C_{Cl^-})^2 C_{Br_2}}{C_{Cl_2}(C_{Br^-})^2}$
K_2	equilibrium constant of Reaction R2, $= \dfrac{C_{HBrO} C_{H^+} C_{Br^-}}{C_{Br_2}}$
K_3	equilibrium constant of Reaction R3, $= \dfrac{C_{BrCl} C_{Br^-}}{C_{Br_2} C_{Cl^-}}$
K_4	equilibrium constant of Reaction R4, $= \dfrac{C_{BrCl_2^-}}{C_{BrCl} C_{Cl^-}}$
K_5	equilibrium constant of Reaction R5, $= \dfrac{C_{Br_2Cl^-}}{C_{Br_2} C_{Cl^-}}$
K_6	equilibrium constant of Reaction R6, $= \dfrac{C_{Br_3^-}}{C_{Br^-} C_{Br_2}}$
K_7	equilibrium constant of Reaction R7, $= \dfrac{C_{HClO} C_{H^+} C_{Cl^-}}{C_{Cl_2}}$
K_8	equilibrium constant of Reaction R8. $= \dfrac{C_{Cl_3^-}}{C_{Cl^-} C_{Cl_2}}$
k	first order reaction rate constant based on electrode surface area (cm s^{-1})

* Present address: Occidental Chemical Corporation, 2801 Long Road, Grand Island, NY 14072, USA.
‡ To whom correspondence should be addressed.

0021-891X

k_m mass transfer coefficient ($cm\,s^{-1}$)
k_{r1} bromide oxidation rate constant ($mA\,cm^{-3}\,M^{-1}$)
k_{r2} chloride oxidation current density ($mA\,cm^{-3}$)
L electrode length (cm)
$(r_{Br^-})_1$ rate of bromide depletion by Reaction R1 ($mmol\,s^{-1}\,cm^{-3}$)
$(r_{Br^-})_2$ rate of bromide generation by Reaction R2 ($mmol\,s^{-1}\,cm^{-3}$)
$(r_{Br^-})_3$ rate of bromide generation by Reaction R3 ($mmol\,s^{-1}\,cm^{-3}$)
v_0 superficial flow velocity ($cm\,s^{-1}$)
y electrode dimension in flow direction (cm)

Greek symbols

ϵ void fraction of porous electrode
ν kinematic viscosity ($cm^2\,s^{-1}$)
ψ molar concentration of BrCl as a function of bromide concentration
Φ overall current efficiency
Φ_{est} current efficiency estimated from theory
Φ_{exp} current efficiency obtained from experiments

Superscripts

0 total
1 inlet
2 outlet
v volume

Subscripts

1,2,3,4,5,6,7,8 Reactions R1 to R8, respectively

1. Introduction

Bromine and its compounds are widely utilized in the photography industry, as sanitation disinfectants, and in manufacturing fire retardants and distinguishing materials, etc. The major means to obtain bromine is its recovery either from natural brine solutions (including sea water, spring water, underground brine, or end liquor from salt manufacture) or from byproduct bromides such as those obtained in halogen displacement reactions. The first one, namely recovery of bromine from brine solutions, constitutes the primary source for bromine since the byproduct bromides originally also come from the brine solutions. Therefore, technologies for efficient bromide recovery have long been sought and many of them are still being explored.

Most of the current commercial technologies are based on a chlorination process in which a bromide-containing brine is fed downward into a packed tower and chlorine gas is countercurrently blown through to drive the following reaction:

$$2Br^- + Cl_2(aq) \rightleftharpoons Br_2(aq) + 2Cl^- \qquad K_1 = 3 \times 10^{10} \qquad (R1)$$

where K_1 is the equilibrium constant at 25 °C. The elemental bromine, having its boiling point near 60°C, can be readily stripped out by steam or blown out by air [1]. Partial or entire stripping can be staged within a same unit by feeding both steam and chlorine gas simultaneously. Alternatively, recovery of elemental bromine can be accomplished by a direct electrochemical route. The advantages of this approach have been outlined previously [2].

Implementation of the electrochemical technology is usually based on a divided cell configuration in which cathode and anode compartments are separated by a diaphragm to eliminate loss of current efficiency due to cathode reduction of bromine generated at the anode. In such a cell, a bromide-rich brine solution flows upward through the anode compartment where the bromide is being oxidized. (Generation of chlorine and oxygen also may occur at the anode when it is subjected to sufficiently positive potential. Whereas the *in situ* generated chlorine reacts instantaneously with bromide in accordance with Reaction R1 and actually enhances electrode utilization, the oxygen generation not only results in extra electricity consumption but also erodes the graphite anode and therefore should be minimized.) The bromine in the anode effluent can be collected by stripping and the spent brine can then be fed to the cathode where oxidized species are reduced and hydrogen is generated by water reduction. A possible process configuration based on this concept is given in Fig. 1.

Problems encountered in developing a commercial electrochemical technology by early pioneering workers included poor performance of the cell separator and low current density owing to dilute bromide concentration in natural brine solutions [1]. The separator performance has been drastically improved as advanced polymeric materials became available. The low current density limit can be overcome by utilizing a three-dimensional electrode. This type of electrode offers large surface area within a compact volume and therefore larger currents may be obtained from

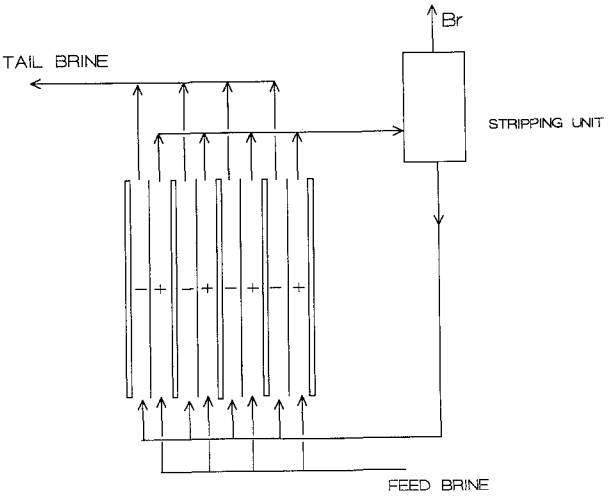

Fig. 1. A flow-through cell stack configuration for bromide recovery from brine solutions.

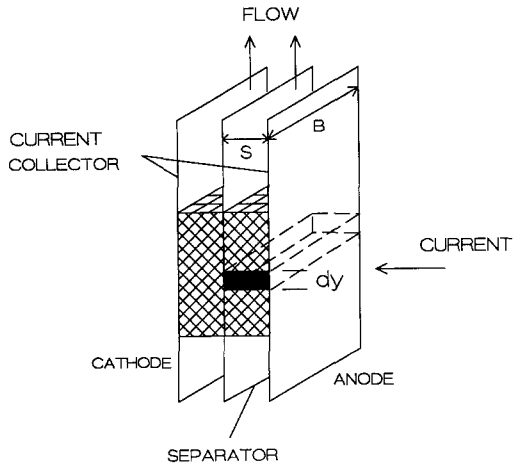

Fig. 2. A differential element of the porous anode.

a small unit despite actual low current density based on the real electrode area. The mass transfer of reactants from bulk electrolyte to the reaction sites also can be greatly enhanced by utilizing a flow-through electrode configuration.

This paper describes recent work on development of such an electrochemical bromide process. In a previous paper [2] we developed a process model to identify the critical factors influencing the cell performance. That paper was aimed at achieving insight into the process characteristics so that the significance of each process variables could be understood. In this paper the feasibility of utilizing this technology under various scenarios are assessed from a more practical cell design point of view. Specifically, we focus on examining the dependence of bromide conversion on the anode length at various flow velocities and anode potentials (which is associated with the anode surface activity). The model reported in [2] serves as a foundation for such analysis. The only prerequisite for using the model to compute the anode length under various operating conditions is an expression for the anode electrochemical kinetics. Consequently, experiments were designed and performed to obtain the kinetic data. The model calculations were then compared with experimental data collected from a pilot cell.

2. Theory and model

The electrolytic cell configuration was composed of graphite felt electrodes placed in two thin channels (about 0.2 cm thick) separated by a permeable polymer membrane. In the laboratory study, two synthetic brine solutions were used separately as anolyte and catholyte, with only the anolyte containing bromide. The direction of electric current was perpendicular to the vertical electrolyte flow. A simplified sketch of the cell is shown in Fig. 2.

2.1. Model development

The earlier model [2] was derived by establishing a mass balance equation for a particular species over a differential length of the anode (see Fig. 2). The mass balance took into account not only the electrochemical reactions but also the homogeneous chemical reactions in the electrolyte phase, which include Reaction R1 and the following:

$$Br_2(aq) + H_2O \rightleftharpoons H^+ + Br^- + HBrO \quad K_2 = 5.8 \times 10^{-9} \quad (R2)$$
$$Br_2(aq) + Cl^- \rightleftharpoons BrCl(aq) + Br^- \quad K_3 = 0.00012 \quad (R3)$$
$$BrCl(aq) + Cl^- \rightleftharpoons BrCl_2^- \quad K_4 = 5.3 \quad (R4)$$
$$Br_2(aq) + Cl^- \rightleftharpoons Br_2Cl^- \quad K_5 = 1.42 \quad (R5)$$
$$Br_2(aq) + Br^- \rightleftharpoons Br_3^- \quad K_6 = 20.2 \quad (R6)$$
$$Cl_2(aq) + H_2O \rightleftharpoons H^+ + Cl^- + HClO \quad K_7 = 4.8 \times 10^{-4} \quad (R7)$$
$$Cl_2(aq) + Cl^- \rightleftharpoons Cl_3^- \quad K_8 = 0.13 \quad (R8)$$

where K_2 to K_8 are the equilibrium constants at 25 °C. Instantaneous equilibrium can usually be assumed in these reactions [2].

The Br^- mass balance can be written as:

$$v_0 \frac{dC_{Br^-}}{dy} = -\frac{a}{F} i_{Br^-} + \epsilon[-(r_{Br^-})_1 + (r_{Br^-})_2 + (r_{Br^-})_3] \quad (1)$$

where v_0 is the superficial flow velocity obtained by dividing anolyte volumetric flow rate by the cross sectional area of the anode channel; a is the specific active surface area of the anode; i_{Br^-} is the current density of electrolytic oxidation of bromide based on the active surface area. Since i_{Br^-} is chosen to be positive, a negative sign appears on the right hand side of Equation 1 to indicate that Br^- is actually consumed by the electrolysis. The terms, $(r_{Br^-})_1$, $(r_{Br^-})_2$, and $(r_{Br^-})_3$, are the rates of bromide generation by Reactions R1, R2, and R3, respectively. A negative sign is also added to the term $(r_{Br^-})_1$ to indicate that bromide is consumed when Reaction R1 proceeds from left to right. In establishing Equation 1 the bromide transport across the membrane cell separator is neglected.

Similarly, separate mass balance equations for species Cl_2, HBrO, BrCl, $BrCl_2^-$, HClO, and Cl_3^- can be established. These equations, combined with Equation 1 and rearranged, produce

$$\frac{dC_{Br^-}}{dy} = -\frac{a}{v_0}\frac{i_{Br^-} + i_{Cl^-}}{F} + 2\frac{dC_{Cl_2}}{dy} + \frac{dC_{HBrO}}{dy} + \frac{dC_{BrCl}}{dy} + \frac{dC_{BrCl_2^-}}{dy} + 2\frac{dC_{HClO}}{dy} + 2\frac{dC_{Cl_3^-}}{dy} \quad (2)$$

where i_{Cl^-} is the current density attributed to chlorine generation. The assumptions used in deriving Equation 2 are: (i) transport of charge carriers, Na^+ and Cl^-, across the cell separator is the only mass transport between the anode and the cathode, and (ii) diffusion in the liquid flow direction is negligible.

Based on the assumption that the homogeneous reactions involving the species shown in Equation 2 are always near or at equilibrium, the concentrations of these species can be shown to be a function of Br^- only. By using the equilibrium relationships, expressions for C_{Cl_2}, $C_{Cl_3^-}$, C_{HBrO}, C_{HClO}, C_{BrCl}, and

$C_{BrCl_2^-}$ as a function of C_{Br^-} can be derived. Subsequently, Equation 2 can be written as

$$(1+h_1+h_2+h_3)\frac{dC_{Br^-}}{dy} = -\frac{a}{v_0}\frac{i_{Br^-}+i_{Cl^-}}{F} \quad (3)$$

where h_1, h_2 and h_3 represent the effects of chlorination, hydration, and BrCl formation, respectively; and are given by:

$$\begin{aligned} h_1 &= -2\frac{dC_{Cl_2}}{dC_{Br^-}} - 2\frac{dC_{Cl_3^-}}{dC_{Br^-}} \\ &= -(1+K_8C_{Cl^-})\frac{2C_{Cl^-}}{K_1K_3C_{Br^-}}\left[\psi' - \frac{\psi}{C_{Br^-}}\right] \end{aligned} \quad (4)$$

$$\begin{aligned} h_2 &= -\frac{dC_{HBrO}}{dC_{Br^-}} - 2\frac{dC_{HClO}}{dC_{Br^-}} \\ &= -\left[1+\frac{2K_7C_{Cl^-}}{K_1K_2C_{Br^-}}\right]\frac{dC_{HBrO}}{dC_{Br^-}} + 2\frac{K_7C_{Cl^-}C_{HBrO}}{K_1K_2(C_{Br^-})^2} \end{aligned} \quad (5)$$

$$h_3 = -\frac{dC_{BrCl}}{dC_{Br^-}} - \frac{dC_{BrCl_2^-}}{dC_{Br^-}} = -(1+K_4C_{Cl^-})\psi' \quad (6)$$

In these equations, ψ represents C_{BrCl} obtained as a function of C_{Br^-} by solving the following two equations:

$$\begin{aligned} &\left[\frac{3K_6}{K_3C_{Cl^-}}(C_{Br^-})^2 + \left(\frac{2}{K_3C_{Cl^-}} + \frac{2K_5}{K_3}\right)C_{Br^-}\right. \\ &\left. + K_4C_{Cl^-} + 1\right]C_{BrCl} = C^0_{Br} - C_{Br^-} - C_{HBrO} \end{aligned} \quad (7)$$

$$\begin{aligned} C_{HBrO} = {} & \frac{K_1K_2C_{Br^-}}{2(K_1K_2C_{Br^-} + K_7C_{Cl^-})} \cdot \\ & \times \left\{\left[(C^1_{H^+} - C^1_{HBrO} - C^1_{HClO})^2\right.\right. \\ & \left.\left. + \frac{4C_{BrCl}}{K_3}\left(\frac{K_2}{C_{Cl^-}} + \frac{K_7}{K_1C_{Br^-}}\right)\right]^{1/2}\right. \\ & \left. - (C^1_{H^+} - C^1_{HBrO} - C^1_{HClO})\right\} \end{aligned} \quad (8)$$

where the superscript 1 denotes the concentrations of the anode influent which are known quantities. C_{HBrO} and dC_{HBrO}/dC_{Br^-} can also be obtained from these two equations. Equation 3, coupled with Equations 4 to 8, governs the anode behaviour and can be used to calculate current efficiency and the required anode length under various operating conditions.

h_1, h_2, and h_3 are functions of C_{Br^-} only (chloride concentration can be considered constant throughout the system). The impact of HBrO on the electrochemical bromide process has been discussed in [2]. In an acidic solution, concentrations of HBrO and HClO are negligibly low and $h_2 \to 0$, whereas h_1 can be disregarded when bromide conversion is below 95% [2].

2.2. Current efficiency

Energy efficiency is largely dictated by the current efficiency associated with producing a given amount of bromine. When the anode potential is sufficiently positive, water oxidation occurs, in addition to generation of bromine and chlorine. The cell current efficiency based on bromide converted at the anode is

$$\Phi = -\frac{Fv_0}{a}\frac{\int_{C^1_{Br^-}}^{C^2_{Br^-}} dC_{Br^-}}{\int_0^L (i_{Br^-} + i_{Cl^-} + i_{O_2})dy} \quad (9)$$

or

$$\Phi = Fv_0SB\frac{C^1_{Br^-} - C^2_{Br^-}}{I} \quad (10)$$

where the numerator in this equation represents the theoretical equivalent current required for the anode to electrochemically convert bromide from the inlet concentration $C^1_{Br^-}$ to the outlet concentration $C^2_{Br^-}$; the denominator is the total current actually consumed, measurable in experiments. Equation 10 is the working equation used to obtain the actual current efficiency after the total cell current and the inlet and outlet bromide concentrations are measured.

Substituting Equation 3 into Equation 9 gives

$$\Phi = \frac{\int_{C^2_{Br^-}}^{C^1_{Br^-}} dC_{Br^-}}{\int_{C^2_{Br^-}}^{C^1_{Br^-}} (1+h_1+h_2+h_3)dC_{Br^-} + \frac{a}{Fv_0}\int_0^L i_{O_2}dy} \quad (11)$$

Clearly the current efficiency is adversely affected by water oxidation (i_{O_2}) as well as the homogeneous reactions represented by h_1, h_2, and h_3. Although oxygen evolution at the anode can be carefully avoided by controlling the anode potential, the current efficiency loss due to h_1, h_2, and h_3 is controlled inherently by the chemical equilibrium. It is evident that a current efficiency of 100% is possible only under conditions where h_1, h_2, and h_3 are zero.

Since i_{O_2} should be independent of y, Equation 11 can be integrated, after substituting h_1 to h_3 by Equations 4 to 6, to yield

$$\begin{aligned} \Phi = -\Delta C_{Br^-}\Bigg(& -\Delta C_{Br^-} + \Delta C_{BrCl} + \Delta C_{BrCl_2^-} \\ & + 2(\Delta C_{Cl_2} + \Delta C_{Cl_3^-} + \Delta C_{HClO}) + \Delta C_{HBrO} \\ & + \frac{I_{O_2}}{Fv_0B}\Bigg) \end{aligned} \quad (12)$$

where Δ denotes concentration change (outlet concentration minus inlet concentration).

The treatment here defines the current efficiency in terms of bromide conversion instead of bromine yield, because the latter also depends on the stripping efficiency for bromine collection as illustrated in Fig. 1. If all bromine, as well as that present in BrCl and $BrCl_2^-$, can be fully recovered and the loss of bromine due to such compounds as HBrO and BrCl is insignificant, the bromine yield is essentially identical to the bromide conversion.

2.3. Anode design

A major variable in feasibility studies or for design considerations is the cell dimension (in particular its length) needed for a given bromine production rate. The cell stacks make up a major capital investment and their dimensions affect the selection of materials of cell construction as well as the design of other peripheral units. For example, the anode–cathode separator must withstand any pressure difference between the two compartments and the entire cell backing plates have to endure the pressure exerted when electrolyte is forced through the porous media. Moreover, the electrolyte flow pattern depends on the cell geometry and the pressure. Therefore, the cell flow distributor design may be affected by pressure and flow velocity. These factors are all related to the cell dimensions, which in turn is governed by the target bromide conversion and the brine processing rate.

Rearranging and integrating Equation 3 gives

$$L/v_0 = -F\int_{C^1_{Br^-}}^{C^2_{Br^-}} \frac{1+h_1+h_2+h_3}{a(i_{Br^-}+i_{Cl^-})}\,dC_{Br^-} \qquad (13)$$

Evidently, when the inlet and outlet bromide concentrations are specified, integrating this equation will give values of the anode length at various flow velocities. The integration can also produce the concentration profile of bromide and other species along the anode length, based on which the current distribution may be calculated. Equation 13 indicates that a larger surface area and a greater chlorine generation permit shorter electrodes for a given bromide conversion. On the other hand, the term, $1+h_1+h_2+h_3$, is greater than unity and increases with bromide conversion [2]. Therefore, the anode length for a given bromide conversion is increased by the homogeneous reactions.

When bromide oxidation is a first order reaction or is controlled by mass transfer, the cell current can be expressed as

$$i_{Br^-}+i_{Cl^-} = Fk_mC_{Br^-}+i_{Cl^-} \qquad (14)$$

where k_m is either the first order reaction constant or the mass transfer coefficient for bromide ions. The mass transfer coefficient may be obtained by experiments or from established correlations. The value of i_{Cl^-} can be regarded as invariable at a fixed anode potential. With a known surface area, a, (which can be measured or estimated), Equation 13, in conjunction with Equation 14, can be integrated to yield the anode length required for various bromide conversions.

If bromide oxidation is controlled by surface kinetics, then i_{Br^-} as a function of bromide concentration and anode overpotential must be known. However, it is usually difficult to obtain the true current density as defined by i_{Br^-} and i_{Cl^-}, which are based on the actual electrochemically active surface area. Therefore, it is convenient to lump current density together with the specific surface area. That is,

$$^vI_{Br^-} = ai_{Br^-} \qquad (15)$$

$$^vI_{Cl^-} = ai_{Cl^-} \qquad (16)$$

Then Equation 13 becomes

$$L/v_0 = -F\int_{C^1_{Br^-}}^{C^2_{Br^-}} \frac{1+h_1+h_2+h_3}{^vI}\,dC_{Br^-} \qquad (17)$$

where ^vI is the total volume cell current density based on unit volume of electrode, which is readily measurable by experiments.

3. Experimental details

3.1. Kinetic measurements

Equation 17 dictates the relationship among bromide conversion, cell current, flow velocity and anode length, and offers a guideline for selection of electrode materials and designing of cell stacks. But to integrate the equation, ^vI as a function of bromide concentration, as well as anode potential, must be known. Therefore, an experimental kinetic study was focused on determination of this relationship.

Several types of carbon or graphite felts were received from two suppliers. Preliminary electrochemical properties of unit volume of the felts were easily screened by linear voltage–sweep cyclic voltammetry in NaBr/NaCl and Na_2SO_4 solutions. A testing electrode was prepared by dipping the mid section of a strip of felt material (about 6–7 cm long and 1 cm wide) into hot wax while both ends of this section were tightly compressed with clamps to prevent the liquid wax from creeping into the end sections by capillary motion. Once the wax at the mid section solidified by cooling, the void spaces between the felt fibres were filled with wax so that electrolyte in contact with one end of the strip could not creep through to the other end. The waxed section was about 2–3 cm long. One end of the felt strip, being free from any wax contamination, was cut into a tip to a desired size and shape and then immersed into electrolyte, while the other end served as an electrical lead to a potentiostat. The geometry of each testing electrode tip was made approximately the same so that the electrode volume was fixed and the voltammograms obtained could be readily compared with one another. A virgin electrode usually exhibited activity slightly different than an aged one. This change could be ascribed to trace contaminants initially present on the surface of the felt fibres. Therefore, a new working electrode was usually subjected to a number of voltammetric cycles before a steady state polarization curve was recorded.

Selection of a flow-through porous electrode material for bromine applications was based on several considerations, namely, good electrochemical activity with respect to bromide and chloride oxidation, but high overpotential for water oxidation, large specific (electrochemically active) surface area,

strong mechanical strength, and last but not least, its cost. A large void fraction is a positive factor since it exerts less resistance to fluid flow. The graphite felt Grade GH 1/8 inch (3.2 mm) (Fiber Materials, Inc.) exhibits overall good properties and therefore was chosen for further flow cell studies. Other materials either lacked mechanical integrity or exhibited high water oxidation currents. For example, although a carbon felt (Grade CH 1/8 inch, Fiber Materials, Inc.) gave slightly better bromide oxidation current than its graphite counterpart, it also exhibited low water oxidation overpotential. The polarization curves indicated that for the graphite felt, (i.e. Grade GH 1/8 inch) oxidations of bromide, chloride, and water began at approximately 0.85–0.9, 0.95–1.0, and 1.2–1.25 V vs SCE, respectively. In spite of its relatively good electrochemical activity, this type of felt was not originally manufactured as electrode material, but was intended to be used as a high temperature thermal insulating material for industrial applications. Thus it also offered good mechanical integrity and was relatively inexpensive.

A prototype bromide oxidation cell constructed of two flow-through porous electrodes divided by a permeable separator is reported in detail in [2]. That cell assembly was modified here so that the electrochemical activity of a small piece of porous electrode sample could be evaluated (see Fig. 3). The present work was directed towards experiments with the graphite felt (Grade GH 1/8 inch). As shown in Fig. 3, the felt was cut into a 1 cm × 1 cm working anode and then sandwiched between a graphite plate and the cell separator. The thickness (0.2 cm) and length (12 cm) of the flow channel were defined by a Teflon spacer. Thus when placed in the channel, the felt was slightly compressed from its nominal thickness of 0.3 cm to assure good electrical contact. The working anode felt was situated in the middle part of the anode graphite plate. A probe (short thin plastic tubing) connected a reference electrode (SCE) to the anolyte entry point [2]. The area of the graphite plate that was not in contact with the felt was covered with a thin Teflon tape to prevent any electrode reaction from taking place and provided an inert section to eliminate effects from developing flow. The area of the graphite plate exposed to the electrolyte (i.e. the section in contact with the felt) was estimated to be very small compared to the surface area of the felt. Thus its contribution to the cell current was negligible.

The cathode channel was essentially the same except that a 3.5 cm long felt segment was housed there. The cathode was separated from the anode by a Daramic 0.038 cm thick microporous polyethylene membrane (W. C. Grace & Co.). For kinetic measurements, an RDE4 potentiostat (Pine Instruments) was used and the electrolyte flow system was similar to the one described in [2]. The anolyte was prepared by dissolving NaBr of various amounts in 5 M NaCl/0.001 M HCl solutions, whereas the catholyte was just a 5 M NaCl/0.001 M HCl solution. Both the anolyte and the catholyte were heated up to a temperature slightly over 80 °C (by heating the electrolyte reservoirs and the cell inlet tubings [2]). The cell itself was tightly wrapped with a thermal insulation material to minimize the temperature gradient between the inlet and the outlet streams. A thermometer situated at the anolyte outlet monitored its outlet temperature. In all the experiments, the catholyte flow velocity was always adjusted to be equal to the anolyte velocity. The anolyte outlet was constantly inspected to ensure that no oxygen gas bubbles were evolved.

3.2. Experiments with a 45 cm long pilot cell

The kinetic measurements described above provide the essential information for the integration of Equation 17. However, it is desirable to verify model calculations experimentally before the model can be used for industrial cell design. For this purpose, a pilot scale cell with long dimensions was constructed to test the model calculations. The cell structure was similar to that depicted in Fig. 3 except that the channels now could hold felt electrodes as long as 45 cm. The anode and the cathode in this cell were of the same material, i.e. Grade GH 1/8 inch, and each were 45 cm long and 1 cm wide. A model TPS-2000 d.c. power supply (Topward Electric Instruments) was used to provide currents as high as 10 A. Other experimental conditions were the same as before except that the electrolysis was carried out at a constant current mode with the anode potential monitored throughout each run. The experimental current efficiency was obtained using Equation 13 by measuring the cell current while the anolyte inlet and outlet were sampled for determination of bromide concentration. Bromide concentration was analyzed based on the hypochlorite oxidation method [2].

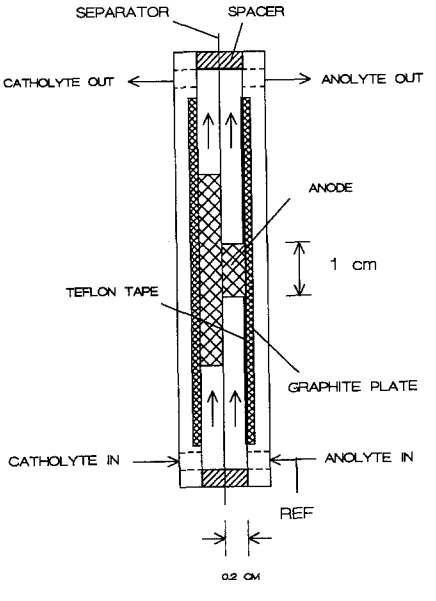

Fig. 3. Schematic diagram of a flow-through porous electrode cell for kinetic measurements.

4. Results and discussion

4.1. Kinetic measurements

Prior to the kinetic measurements, the experimental conditions under which the electrolysis is controlled by surface kinetics must be determined. Several experiments were first carried out using the cell arrangement illustrated in Fig. 3 (namely, the anode was 1 cm long × 1 cm wide graphite felt) to identify the velocity region where the effect of bromide mass transfer from bulk solution to the electrode surface becomes insignificant. This was accomplished by varying the anolyte superficial flow velocity – the catholyte flow velocity was always adjusted to the same value of the anolyte – and subsequently measuring the change in the cell current. Data obtained at a constant anode potential of 1.15 V vs SCE and at various flow velocities ranging from below 0.5 cm s^{-1} to about 6.4 cm s^{-1} showed that the cell current first increased with the superficial flow velocity and then remained constant when the velocity approached 4.5 cm s^{-1}. Further increase of the velocity would not change the cell current. For example, for an anolyte containing 0.01 M NaBr/5 M NaCl/0.001 M HCl, the cell current at 1.15 V vs SCE increased from ≈ 80 to ≈ 100 mA when the velocity was increased from 1 to 4.5 cm s^{-1}, and then was unaffected by further increase in the velocity. If the anolyte contained 0.03 M NaBr/5 M NaCl/0.001 M HCl, the increase in the cell current was from 100 to 130 mA for the same range of velocity but again became virtually unchanged at higher velocities. These results suggest that when the superficial flow velocity is greater than 4.5 cm s^{-1}, the mass transfer coefficient becomes sufficiently large and it no longer affects the surface kinetics. Therefore, most of the kinetic measurements were made with the anode potential below 1.15 V vs SCE and a velocity greater than 4.5 cm s^{-1} so that the current-concentration data reflected purely the characteristics of the surface kinetics.

Table 1 summarizes the currents obtained at various anode potentials, as well as anolyte bromide concentrations, under a constant anolyte flow velocity of 4.8 cm s^{-1}. For a virgin electrode, there usually existed an initial period during which the cell current drifted. The cell current then achieved a final steady state value which was subsequently recorded. In some experiments, after the cell current was recorded, the flow velocity was doubled to ensure that the current still stayed unchanged upon the increase of the velocity.

The fast flow rate and the short length of the testing electrode usually led to a very low bromide conversion and, for high inlet bromide concentrations, resulted in a nearly uniform bromide concentration profile throughout the anode. However, at low inlet bromide concentrations, variation of concentration inside the cell might not be negligible. Nevertheless, the concentration difference between the inlet and outlet streams was estimated from the cell current and the anolyte flow rate by assuming 100% current efficiency. (This assumption is reasonable since in these experiments,

Table 1. Steady state cell currents at different bromide concentrations obtained from Fibre Materials, Inc., GH 1/8 inch graphite felt

Inlet Br^- Concentration (M)	*Run*	*Cell current at different anode potentials (V vs SCE) mA*					
		0.95	*1.00*	*1.05*	*1.10*	*1.15*	*1.20*
0	1	0	6	15	40	84	–
	2	7	12	20	40	85	130
	3	1	4	10	36	84	126
0.010	1	20	31	47	70	103	–
	2	22	33	59	79	104	145
	3	15	30	49	68	102	148
(Average C_{Br^-})/M		*0.0099*	*0.0098*	*0.0097*	*0.0096*	*0.0094*	*0.0092*
0.030	1	36	58	80	102	132	–
	2	38	60	85	105	129	166
	3	32	57	86	115	140	175
(Average C_{Br^-})/M		*0.030*	*0.030*	*0.029*	*0.029*	*0.029*	*0.029*
0.050	1	45	73	105	135	163	–
	1	54	82	110	139	162	204
	3	45	77	108	145	175	216
(Average C_{Br^-})/M		*0.050*	*0.050*	*0.050*	*0.049*	*0.049*	*0.049*
0.070	1	63	95	125	150	190	–
	2	66	98	125	156	188	225
	3	60	95	133	170	210	245
(Average C_{Br^-})/M		*0.070*	*0.070*	*0.069*	*0.069*	*0.069*	*0.069*

Run 1 and run 2: duplicate experiments
Run 3: data obtained using electrode material from a different shipment.
Anolyte flow velocity = 4.8 cm s^{-1}
Electrolyte concentration: NaCl = 5 M; HCl = 0.001 M
Anode dimension: 1 cm long, 1 cm wide, 0.2 cm thick
Temperature = 80 °C.

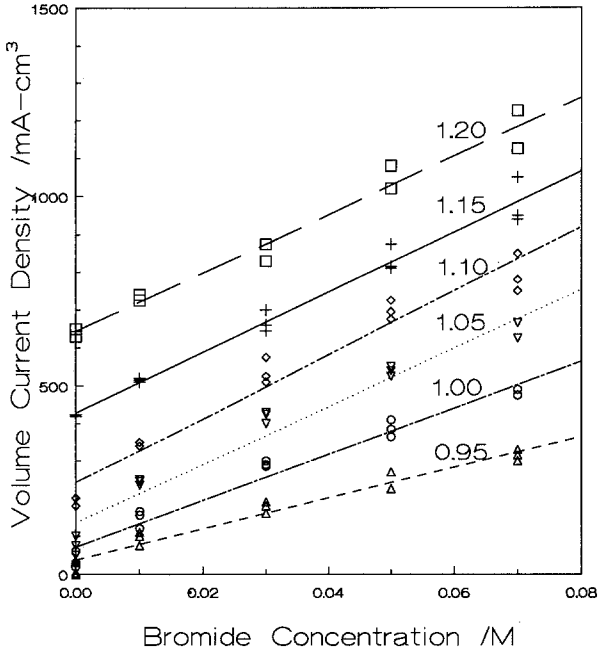

Fig. 4. The linear relationship between the volume current density and bromide concentrations.

bromide conversion at most was about 10%. As concluded in [2], the current efficiency should be near 100% at such a low level of conversion.) The average of the inlet and outlet bromide concentrations was then obtained and the values are included in Table 1. Note that run 2 was simply a repetition of run 1, to show the reproducibility of the experiments. Run 3 was conducted using a graphite felt material of the same type but from a different shipment. As can be clearly seen, the data in run 2 coincided very closely with those from run 1, while run 3 gave slightly higher currents. This may be simply from the small difference between the surface area of these two electrode samples. (The dimensions of the graphite felt were 'soft' dimension whose precise determination was difficult to obtain because of its fuzzy edges.) When the volume current density obtained from the data in Table 1 is plotted against the average bromide concentration (Fig. 4), a linear relationship apparently exists:

$$^{v}I = k_{r1} C_{Br^-} + k_{r2} \tag{18}$$

where k_{r1} is the reaction rate constant for bromide oxidation and k_{r2} is the chloride oxidation current density. The values of the constants regressed from the experimental data are listed in Table 2. It is interesting to note that the slope of the line, i.e. the value of k_{r1}, did not increase further when the anode potential exceeded 1.05 V vs SCE. This was likely due to the decrease of surface area available for bromide oxidation when a large chlorine generation current was present rather than a limiting current. It will be shown in the following paragraphs that this constancy in the slope is not attributable to the effect of mass transfer limiting conditions.

There are a number of publications devoted to measurement and correlation of mass transfer

Table 2. Reaction rate constants obtained from experiments

ϕ_a/V vs SCE	$k_{r1} \times 10^{-3}$/mA cm^{-3} M^{-1}	k_{r2}/mA cm^{-3}
0.95	4.09	37
1.00	6.16	71
1.05	7.73	135
1.10	8.48	242
1.15	7.95	429
1.20	7.70	644

coefficients in a porous media [3, 4]. For example, the correlation of Fenton and Alkire [3] has the following form:

$$\frac{k_m \epsilon}{aD} = 11.0\left(\frac{v_0}{a\epsilon\nu}\right)^{0.3} \tag{19}$$

The viscosity for a 5 M NaCl solution at 80 °C is about 0.7 centipoise and the density is 1.2 g cm^{-3} [5, 6]. The diffusion coefficient of bromide ions in 5 M NaCl solutions is not available but $D = 1 \times 10^{-5}$ cm^2 s^{-1} should be a reasonable approximation for the analysis purpose here. Since the felt electrode had a void fraction greater than 0.8 and its specific surface area typically varied between 150 to 300 cm^{-1} [4], $\epsilon = 0.9$ and $a = 200$ cm^{-1} were chosen as being representative. Using these values and Equation 19, the mass transfer coefficient of bromide ions at a superficial velocity of 4 cm s^{-1} was found to be about 0.04 cm s^{-1}. Correlations from other sources (such as [4]) appear to give similar estimates.

If $k_{r1} = 8 \times 10^3$ mA cm^{-3} M^{-1} as in Table 2 and $a = 200$ cm^{-1}, the reaction rate constant based on the electrode surface area is $k = k_{r1}/aF = 4 \times 10^{-4}$ cm s^{-1}. This is more than two orders of magnitude lower than the estimated mass transfer coefficient, therefore suggesting that the process was not under mass transfer limiting conditions.

Using Equation 18, Equation 17 can be written as

$$L/v_0 = -F\int_{C^1_{Br^-}}^{C^2_{Br^-}} \frac{1 + h_1 + h_2 + h_3}{k_{r1} C_{Br^-} + k_{r2}} \mathrm{d}C_{Br^-} \tag{20}$$

Also, if the bromide conversion, f, is defined as

$$f = \frac{C^1_{Br^-} - C^2_{Br^-}}{C^1_{Br^-}} \tag{21}$$

Equation 20 can be integrated to produce L/v_0 at different anode potentials and for various bromide conversions. Therefore, for a given set of conditions, the cell performance in terms of bromide conversion and brine throughput can be assessed. Or conversely, if a desired bromide conversion and bromine production rate are specified, Equation 20 can be used to guide the designing and scaling up of cell stacks. Calculations for one case where the anolyte stream contains 0.07 M bromide and 5 M NaCl are shown in Fig. 5. The figure clearly indicates that bromide conversion is enhanced by increasing L/v_0 and/or anode potential. If the conversion and the flow velocity are fixed, higher anode potentials will reduce the required anode length. Furthermore, to scale up such a process

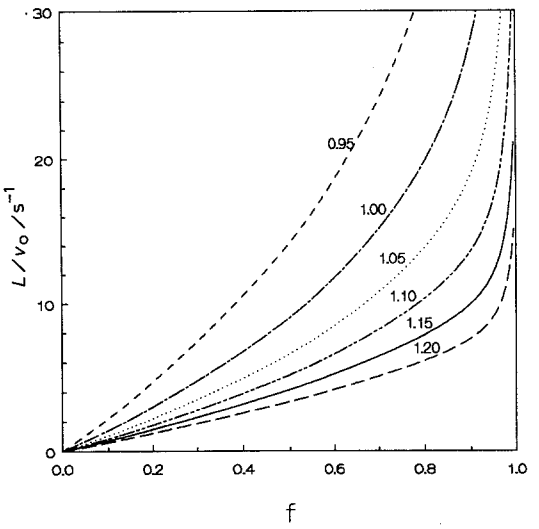

Fig. 5. Ratio of anode length to anolyte flow velocity, L/v_0, calculated as a function of bromide conversion at several anode potentials for $C^1_{Br^-} = C^0_{Br} = 0.07$ M; $C_{Cl^-} = 5$ M; $C^1_{H^+} = 10^{-7}$ M; $C^1_{HBrO} = C^1_{HClO} = 0$.

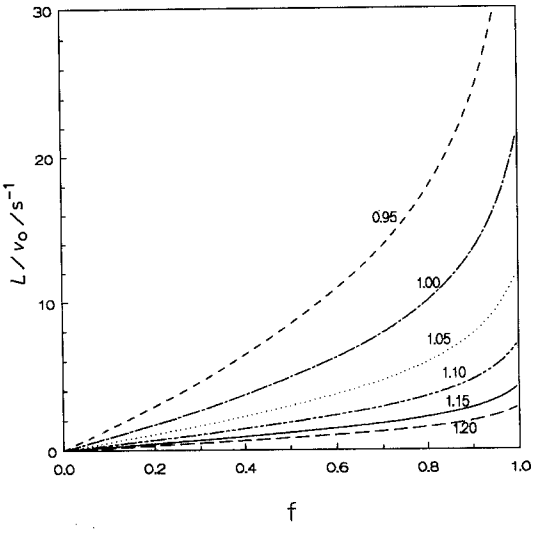

Fig. 6. Ratio of anode length to anolyte flow velocity, L/v_0, calculated as a function of bromide conversion at several anode potentials for $C^1_{Br^-} = C^0_{Br} = 0.01$ M; $C_{Cl^-} = 5$ M; $C^1_{H^+} = 10^{-7}$ M; $C^1_{HBrO} = C^1_{HClO} = 0$.

from a laboratory unit, the critical parameters to consider in order to achieve a comparable bromide conversion is L/v_0 and the anode potential.

To demonstrate the effect of the inlet bromide concentration, calculations for bromide concentration of 0.01 M are plotted in Fig. 6. Comparing Figs 5 and 6 suggests that decreasing inlet bromide concentration surprisingly will reduce the L/v_0 needed to achieve the same bromide conversion. The analysis in [2] indicates that in the absence of chlorine generation, achieving lower bromide concentrations requires longer electrodes owing to the homogeneous reactions. However, this negative effect was overridden here by the presence of chlorine generation, which tended to enhance electrode utilization. The current efficiency, however, declines significantly with the inlet bromide concentration as shown in [2]. An optimum inlet bromide concentration should exist and should depend on a balance between these two factors (i.e. L/v_0 against current efficiency).

4.2. *Verification of predicted anode length*

It is evident that Equation 20 serves as a useful tool in designing and scaling up the electrochemical process for bromide recovery. The reliability of the calculated L/v_0 depends largely on the accuracy of the kinetic data as well as the validity of Equation 20. Therefore, experiments were conducted using a 45 cm long pilot cell to test the model predictions.

A total of twelve runs were conducted with the pilot cell, and the results are reported in Table 3, where the theoretical values of the current efficiency are calculated using Equation 12 with $i_{O_2} = 0$ and the estimated bromide conversions are obtained using Equation 20. The runs were all carried out galvanostatically and only the values at steady state were recorded. Note that the equilibrium constants for the homogeneous reactions at 25 °C were used in the calculations since their values at 80 °C were not available. Interestingly, in many of these runs the actual bromide conversion appeared to be slightly

Table 3. Experimental data obtained using a 45 cm cell compared to theoretically estimated values

Run	$v_0/cm\,s^{-1}$	I/A	ϕ_a/V vs SCE	ΔV/V	$C^1_{Br^-}$/M	$C^2_{Br^-}$/M	f_{exp}	f_{est}	Φ_{exp}	Φ_{est}
L1	6.5	6.0	1.10	–	0.0706	0.0253	0.64	0.62	0.96	0.96
L2	5.2	6.0	1.10	–	0.0706	0.0169	0.76	0.73	0.91	0.94
L3	6.5	6.0	1.10	–	0.0706	0.0268	0.62	0.62	0.93	0.96
L4	3.7	7.0	1.16	2.6	0.0637	0.0009	0.99	0.96	0.64	0.64
L5	4.7	6.8	1.18	2.6	0.0637	0.0025	0.96	0.97	0.82	0.78
L6	4.0	8.0	1.20	–	0.0670	0.0009	0.99	0.98	0.64	0.63
L7	4.5	9.0	1.20	–	0.0670	0.0029	0.96	0.97	0.62	0.79
L8	7.1	9.0	1.20	–	0.0670	0.0100	0.85	0.83	0.87	0.92
L9	3.5	7.5	1.15	2.7	0.0705	0.0003	0.99	0.96	0.63	0.56
L10	4.7	6.8	1.15	2.6	0.0705	0.0034	0.95	0.89	0.90	0.81
L11	4.6	7.2	1.15	2.6	0.0703	0.0034	0.95	0.90	0.82	0.82
L12	4.8	8.0	1.19	2.7	0.0703	0.0036	0.95	0.92	0.78	0.82

Anolyte inlet stream: NaBr/5 M NaCl/0.001 M HCl; anode compartment: 45 cm long, 1 cm wide, 0.2 cm thick. The cathode is identical to the anode; temperature: 80 °C. v_0: anolyte flow velocity (the catholyte had the same flow rate as the anolyte); I: cell current; ϕ_a: anode potential; $C^1_{Br^-}$, $C^2_{Br^-}$: inlet and outlet bromide concentrations; ΔV: cell voltage; f_{exp}, f_{est}: measured and estimated values of bromide conversion; Φ_{exp}, Φ_{est}: measured and estimated values of current efficiency.

better than the predicted values. This perhaps resulted from variability in surface activity and/or electrode dimensions. An electrode felt cut slightly wider could still fit in the 1 cm spacer but would give a larger surface area available for the reactions. Also, the approximation introduced by using the equilibrium constants at 25 °C instead of 80 °C may result in some difference between the calculated and measured values.

Some of the current efficiency data appears to deviate significantly from the predicted values. This can be attributed to the fact that when the bromide conversion exceeded 85%, the current efficiency dropped sharply with the bromide conversion [2]. Therefore, a small variation in the conversion leads to a large change in current efficiency. Also, errors associated with flow and concentration measurements may contribute to these deviations. However, in spite of these deviations, the agreement between actual and predicted performance overall appears to be good.

5. Conclusion

The process model established earlier [2] accounts for the homogeneous reactions and has suggested that lower current efficiency and longer electrodes are a result of these reactions and that the effects become more pronounced when the anolyte bromide level is reduced. This is, however, only partially true with regard to the electrode length since the analysis was made with the assumption of no chlorine generation. The effect of the homogeneous reactions on the cell dimensions can be both positive and negative, depending on the magnitude of chlorine generation. On one hand, bromide oxidation by *in situ* generated chlorine helps to greatly enhance the electrode utilization. But on the other hand, formation of BrCl tends to lower the electrode efficiency and increase the anode length needed for a given bromide feed conversion. For the graphite felt electrode studied, chlorine generation was shown to be abundant and its effect was dominant. Consequently, lower bromide feed concentration actually resulted in better anode performance in terms of higher bromide conversion.

The cell current efficiency was impaired by two effects, namely, water oxidation and homogeneous reactions. While the effect of water oxidation can be minimized by careful selection of electrode material that exhibits high overpotential for water oxidation, acidifying the anolyte stream, and/or good control of the anode potential as has been done here, the adverse effect of the homogeneous reactions is not at all related to the electrode properties and can only be reduced by increasing bromide concentration in the feed brine, or lowering bromide conversion. Low chloride concentration reduces the adverse effect of homogeneous reactions, but diluting a natural brine would reduce bromide cell throughput. The homogeneous reaction equilibrium constants can be affected by system temperature and pressure, which, however, are usually fixed based on other process considerations.

The model equation developed here is useful in highlighting key parameters and in guiding the selection of electrode materials. Experimental kinetic data incorporated into the model allow evaluation of various operating scenarios and may assist in optimizing a bromide recovery process.

Acknowledgement

This work was funded by Great Lakes Chemical Corporation.

References

[1] Z. E. Jolles (Ed.), 'Bromine and its Compounds', Academic Press, New York (1966) pp. 27–29, p. 154 and p. 750.
[2] J. Qi and R. F. Savinell, *J. Appl. Electrochem.* **23** (1993) 873.
[3] J. M. Fenton and R. C. Alkire, *J. Electrochem. Soc.* **135** (1988) 2200.
[4] B. Delanghe, S. Tellier and M. Astruc, *Electrochim. Acta* **35** (1990) 1369.
[5] R. C. Weast and M. J. Astle, (Eds), 'CRC Handbook of Chemistry and Physics', 60th edn, Boca Raton, FA (1979) p. F-11, p. F-51, p. D-262.
[6] R. C. Reid, J. M. Prausnitz, and T. K. Sherwood, 'The Properties of Gases and Liquids', McGraw-Hill, New York (1977) p. 438.